# Theory and Measurement of Back Bias Voltage in IMPATT Diodes

LOWELL H. HOLWAY, JR. AND SHIOU LUNG G. CHU

*Abstract*—**The derivation of the back bias voltage is shown to require carrying the derivation of the Read equation to one order of approximation higher than that which is necessary to obtain the quasi-static result. A new term is shown to be needed in the expression for the back bias voltage which changes its sign to positive under conditions in which the older analyses indicate a negative back bias. Experimental measurements of $V_{bb}$ as a function of $V_{RF}$ were made using a network analyzer and are in agreement with the new analysis. At frequencies considerably below the range at which our measurements were made, a strong negative back bias voltage is caused by the saturation current.**

## I. Introduction

THE BACK BIAS VOLTAGE $V_{bb}$ is the change in the dc voltage across an IMPATT diode due to the RF drive. A negative $V_{bb}$ is known to encourage bias current instabilities [1], [2] and to advance the phase of current injection which tends to reduce the negative conductance [2].

Formulas for $V_{bb}$ based on the standard Read equations have been given by several authors [1]–[3]. For example, Culshaw *et al.* [2] find

$$V_{bb} = -\frac{\alpha''}{4\alpha'}\frac{V_{RF}^2}{w_T^2} \tag{1}$$

where $\alpha'$ and $\alpha''$ are the first and second derivatives of the ionization coefficient with respect to field, $w_T$ is the total width of the depletion regions, and $V_{RF}$ is the peak RF voltage across the diode. The derivatives of $\alpha$ are taken at the breakdown field and, in GaAs, for avalanche widths greater than about 0.25 $\mu$m, $\alpha''$ is positive, so that (1) predicts a negative back bias.

Although a similar expression for back bias was given by Goedbloed [3], his experimental measurements in GaAs were in contradiction to the theory and showed a positive, rather than a negative, back bias. Our observations, reported in Section V, are similar in that they show $V_{bb}$ is positive for a *K*-band double-drift IMPATT diode with an avalanche width of 0.37 $\mu$m.

In addition to these experimental measurements, the "anomalous" back bias voltage has been demonstrated by Blakey *et al.* [4] by means of a numerical computer simulation of an IMPATT diode with a 0.45-$\mu$m avalanche zone. In addition to the anomalous effect, their calculation showed that the back bias became negative again when the frequency was reduced below 10 GHz. Although our measurements were taken at higher frequencies, where the back bias behavior is insensitive to frequency, we will put our results in context by showing that the saturation current causes the back bias voltage to change signs at the lower frequencies.

Although computer simulations of the partial differential continuity equations can calculate the back bias correctly, we would like to understand this theoretically by using the Read equation. We will show that this requires deriving the Read equation to one order of approximation higher than is customary. This higher order term can be understood to cause an effective modulation of the avalanche response time $\tau_l$. In fact, $\tau_l$ is equal to the quasi-static value of 1/3 the avalanche zone transit time only when $\alpha l = 1$, and is larger when $\alpha l$ exceeds one. For an IMPATT diode, this means that the avalanche current increases at a slightly slower rate, while $\alpha l$ is greater than unity, than it decreases when $\alpha l$ is less than unity. In order to maintain a steady dc current, the net increase in current over a cycle must vanish, so the average or dc value of $\alpha l$ must exceed unity; that is, $V_{bb}$ must be positive. This effect is entirely analagous to the effect of a positive value of $\alpha''$, which causes the avalanche current to increase too rapidly when $\alpha l$ is greater than one and therefore requires a negative back bias voltage.

In Section II, the Read equation will be derived in the quasi-static approximation. Then a consistent formalism will be introduced in Section III which allows the approximation to the Read equation to be carried out to an arbitrarily high order. In Section IV, the back bias voltage is derived from this modified Read equation. Experimental measurements of $V_{bb}$ on a *K*-band double-drift GaAs IMPATT diode are described in Section V, and compared with the theory we have developed. Low frequency effects due to the saturation current are described in Section VI.

## II. Derivation of the Read Equation

For GaAs IMPATT diodes, it is a good approximation to assume equal ionization coefficients, $\alpha = \beta$, and equal carrier velocities $v_n = v_p$. For the EHF diodes that we will consider, the saturation current can be neglected since the dc current density $J(t) \gg J_{sat}$ at all times. We make these simplifications here, since it would only lengthen the algebra to treat a more general case, even though there would be no real difficulty in doing that.

Manuscript received October 19, 1982; revised July 11, 1983.

The authors are with the Raytheon Research Division, Lexington, MA 02173.

0018-9480/83/1100-0916$01.00 ©1983 IEEE

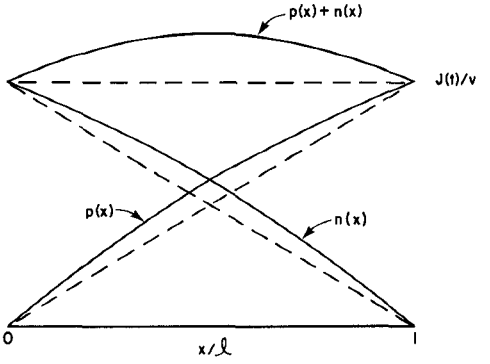


Fig. 1. Schematic plots of carrier densities and current versus position. The dashed lines, indicating the solution when $\alpha l = 1$, are modified as indicated by the solid curves for $\alpha l$ greater than unity.

Since the current density is dependent on position, for preciseness, we will define $J(t)$ as the current leaving the avalanche at the particular position $x = l$. For simplicity, it is convenient to choose units in which the charge $q = 1$. Then, neglecting the saturation current density, the hole and electron densities $p$ and $n$ are shown schematically in Fig. 1. These carrier densities satisfy the boundary conditions

$$p(0) = n(l) = 0 \tag{2a}$$

and

$$p(l) = n(0) = J(t)/v \tag{2b}$$

where the equality of $p(l)$ and $n(0)$ is a result of the symmetry when $\alpha = \beta$ and $J_{sat} = 0$. The current densities satisfy the continuity equations

$$\frac{\partial p}{\partial t} + v\frac{\partial p}{\partial x} = \alpha v(n+p) \tag{3a}$$

and

$$\frac{\partial n}{\partial t} - v\frac{\partial n}{\partial x} = \alpha v(n+p). \tag{3b}$$

In this analysis, we treat $\alpha$ as a constant across an avalanche zone of width $l$. Now let $\alpha l = 1 + \delta$, so that the solution approaches a steady state when the small parameter $\delta$ approaches zero. Following Read [5], we add (3a) and (3b) and integrate from 0 to $l$, giving

$$\frac{\partial Q}{\partial t} + 2J(t) = 2(1+\delta)vQ/l \tag{4}$$

where

$$Q = \int_0^l (n+p)\,dx = lJ(t)/v + \delta Q_1(x,t)$$

and the expansion for $Q$ $(= Q_0 + \delta Q_1 + \cdots)$ has taken into account the fact that the current is independent of position when $\delta = 0$. Then, keeping terms of order $\delta$, (4) becomes

$$\frac{l}{2v}\frac{\partial J}{\partial t} = (\alpha l - 1)\left[J + \frac{v}{l}Q_1\right]. \tag{5}$$

If $Q_1$ were taken to be zero, (5) would give Read's original equation with $\tau_t = \frac{1}{2}l/v$. However, we will now evaluate $Q_1$, taking the difference of (3a) and (3b), to get

$$\frac{\partial}{\partial x}(p+n) = \frac{1}{v}\frac{\partial}{\partial t}(n-p). \tag{6}$$

To proceed, we invoke the quasi-static approximation for the slowly varying quantities on the right-hand side of (6). This approximation, given by the dashed line in Fig. 1, means that, in the lowest order approximation

$$n - p = \frac{1}{v}(1-2x/l)J(t). \tag{7}$$

Next, using (7) to integrate (6) twice gives

$$\delta Q_1 = \frac{1}{6}\frac{l^2}{v^2}\frac{\partial J}{\partial t}$$

so that (5) becomes the quasi-static Read equation

$$\frac{1}{3}\frac{l}{v}\frac{\partial J}{\partial t} = (\alpha l - 1)J. \tag{8}$$

The approximation taking advantage of the slowly varying right-hand side of (6) is essential in the quasi-static method introduced by Kuvas and Lee [6], although the approach taken here shows that it is unnecessary to introduce the displacement current as they did in carrying through the approximation. The key part in obtaining $\tau_t = \frac{1}{3}l/v$ is to recognize that $(\alpha l - 1)J(t)$ and $\delta Q_1$ are both of first order in $\delta$, so that $Q_1$ cannot be ignored in (5).

## III. High-Order Solutions of the Read Equation

To obtain the higher order solutions which are needed for the back bias problem, we will introduce a more formal expansion

$$vp(x,t) = J(t)\sum_{m=0}^{\infty} p_m(x)\delta^m \tag{9a}$$

$$vn(x,t) = J(t)\sum_{m=0}^{\infty} n_m(x)\delta^m \tag{9b}$$

and

$$\frac{l}{3v}\frac{\partial J}{\partial t} = J(t)\sum_{m=1}^{\infty} a_m\delta^m \tag{10}$$

where $a_m$, $p_m(x)$, and $n_m(x)$ are considered dimensionless variables of order unity. Substituting (9) and (10) into (3a) and (3b), and ignoring terms proportional to $\delta$, yields what we previously called the quasi-static approximation for the carrier densities, namely

$$p_0(x) = x/l \tag{11a}$$

and

$$n_0(x) = 1 - x/l. \tag{11b}$$

For higher order solutions, the boundary conditions require $p_m(0) = p_m(l) = n_m(0) = n_m(l) = 0$. An algorithm to determine these functions is obtained by assuming that we know $p_m$, $n_m$, and $a_m$ for $m = j$, and using these functions to determine the next higher order terms for $m = j+1$. This algorithm is developed by taking the difference of (3a) and (3b), which, as in (6), gives the expres-

sion

$$\frac{\partial}{\partial x}(p_{j+1}+n_{j+1})=\frac{3}{l}\sum_{m=1}^{j+1}a_m(n_{j+1-m}-p_{j+1-m}) \quad (12)$$

where (12) includes all terms of order $j+1$. Next, (3a) and (3b) are added and integrated from 0 to $l$ to obtain, as in (4), the expression

$$\frac{3}{2}\sum_{m=1}^{j+1}a_m\int_0^l(n_{j+1-m}+p_{j+1-m})\,dx = \int_0^l(p_{j+1}+n_{j+1}+p_j+n_j)\,dx \quad (13)$$

which again includes all terms of order $j+1$. After integrating (12) twice in order to eliminate

$$\int_0^l(p_{j+1}+n_{j+1})\,dx$$

from (13), the resulting equation can be solved for $a_{j+1}$, and which determines the modified Read equation, (10), through terms of order $j+1$.

The solution for $p_{j+1}(x)$ can be obtained by writing the terms of order $j+1$ in the original continuity equation, (3a) which yields

$$l\frac{\partial p_{j+1}(x)}{\partial x}=p_{j+1}(x)+n_{j+1}(x)+p_j(x)+n_j(x) -3\sum_{m=1}^{j+1}a_m p_{j+1-m}(x) \quad (14)$$

where, since all terms on the right-hand side of (14) are known when $p_{j+1(x)}+n_{j+1(x)}$ is obtained by integrating (12) once, $p_{j+1}(x)$ is obtained by integrating (14) using the boundary condition $p_{j+1}(0)=0$. In the same way, $n_{j+1}(x)$ is obtained from (3b), which takes on the form

$$l\frac{\partial n_{j+1}(x)}{\partial x}=-p_{j+1}(x)-n_{j+1}(x)-p_j(x)-n_j(x) +3\sum_{m=1}^{j+1}a_m n_{j+1-m}(x). \quad (15)$$

The expansions of (9) and (10) can be shown to satisfy (3a) and (3b), the continuity equations, at each successive power of $\delta$. The terms through $j=2$ which are required to determine the back bias voltage are listed in Table I. The functions $p_n+n_n$, which specify the conduction current in the avalanche zone, are plotted in Fig. 2, through the second order of approximation.

Equation (10) has the standard form of the Read equation

$$\tau_l\frac{\partial J}{\partial t}=(\alpha l-1)J(t) \quad (16)$$

where

$$\tau_l=\frac{1}{3}\frac{l/v}{\sum_{m=1}^{\infty}a_m\delta^{m-1}}\cong\frac{1}{3}\frac{l}{v}\left(1+\frac{1}{5}\delta\right) \quad (17)$$

where Table I has been used to express $\tau_l$ to the level of approximation needed in the next section.

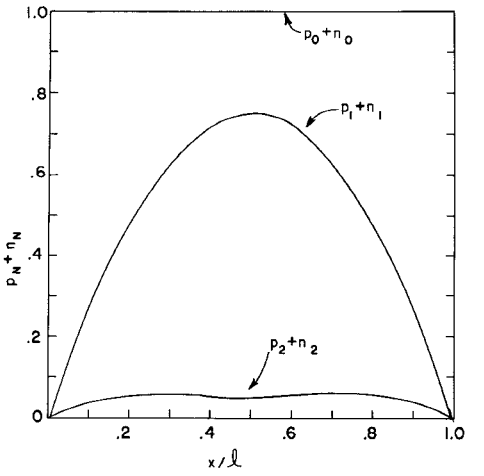


Fig. 2 Current density versus position. The coefficients of the first few powers of $\delta$ in the current density expansion are shown.

TABLE I
EXPANSION COEFFICIENTS FOR CARRIER DENSITIES

| m | $p_m$ | $n_m$ | $a_m$ |
|---|---|---|---|
| 0 | $x/\ell$ | $1-x/\ell$ | --- |
| 1 | $x/\ell\,(1-x/\ell)\,(1+x/\ell)$ | $\frac{x}{\ell}(1-\frac{x}{\ell})\,(2-x/\ell)$ | 1 |
| 2 | $-\frac{3}{10}\frac{x^3}{\ell^3}(1-x/\ell)\,(1+x/\ell)$ | $-\frac{3}{10}\frac{x}{\ell}(1-x/\ell)^3\,(2-x/\ell)$ | -1/5 |

A completely independent derivation of $\tau_l$ can be based on an eigenfunction expansion that we have described in [7]. In that reference, it was shown that, for $\alpha=\beta$, the most rapidly growing eigenfunction increased as $\exp(v_s\alpha\lambda t)$ where $v_s=2v_nv_p/(v_n+v_p)$. Here $v_s$ equals $v$ when the carrier velocities are equal so that $v_n=v_p=v$. The eigenvalue $\lambda$, for $\alpha=\beta$, was shown to satisfy the equations

$$1-\lambda=\kappa\cot\kappa\alpha l \quad (18)$$

and

$$\kappa=\sqrt{2\lambda-\lambda^2} \quad (19)$$

where, by comparison with (16), we find

$$\tau_l=(\alpha l-1)/\lambda\alpha v_s. \quad (20)$$

An expansion of (18)–(20) in powers of $\delta$ agrees term by term with the expansion developed in this paper. In Fig. 3, the numerical solution for $\tau_l/\tau_{\text{transit}}$ from (18)–(20) is plotted as a solid curve versus $\alpha l$, while the first two terms of the power series in (17) are shown as the dashed straight line. It can be concluded that these terms give an excellent solution over the range of $\alpha l$ involved in IMPATT diode operations.

Although we are interested in an experimental situation where $\alpha\cong\beta$ and $v_n\cong v_p$, so that (17) applies, the results of [7] provide a convenient way to generalize the calculation when $\alpha\neq\beta$. Similarly, both in theory and in our experimental situation, we assumed $J(t)\gg J_{\text{sat}}$. However, (16) can be generalized in the same way as the original Read equation to give

$$\tau_l\frac{\partial J}{\partial t}=(\alpha l-1)\left(J(t)+\frac{J_{\text{sat}}}{\alpha l-1}\right) \quad (21)$$

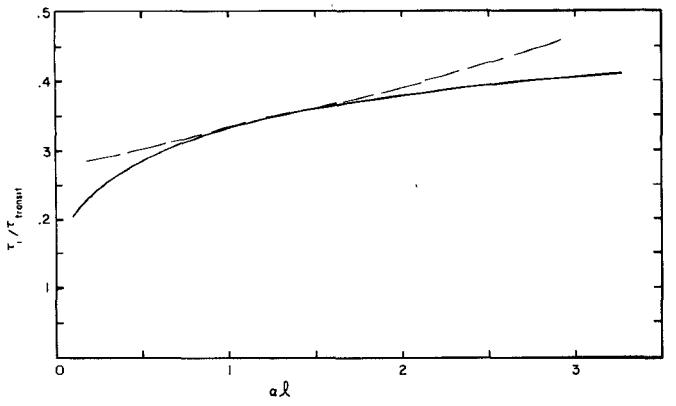


Fig. 3. Avalanche response time as a function of $\alpha l$. The solid curve is a numerical solution of the eigenvalue equations, while the dashed line is the linear term in the expansion in powers of $\alpha l - 1$. The response time is normalized by $\tau_{transit} = l/v$.

where $J$ is now the total current at $x = l$, that is, $J = vp(l) + vn(l) = vp(l) + J_{ns}$ where $J_{sat} = J_{ns} + J_{ps}$.

## IV. Magnitude of the Back Bias Voltage

From (16), the current density satisfies

$$J(t) = J_0 \exp \int_0^t \frac{(\alpha l - 1)}{\tau_i} dt \tag{22}$$

where the electric field in the avalanche zone is assumed to satisfy

$$E = E_0 + E_{RF} \sin \omega t. \tag{23}$$

If (22) is to be periodic, the integral over a period must vanish, that is

$$\int_0^T (\alpha l - 1)(1 - \delta/5)\, dt = 0 \tag{24}$$

where $\omega T = 2\pi$ and the $\delta/5$ term is introduced because $\tau_i$ is no longer a constant. Notice that we are treating $\alpha$ as a function of time, even though our original derivation kept $\alpha$ constant. This "adiabatic" approximation is generally appropriate for IMPATT diodes in which the logarithmic rate of change $\alpha$ is small compared to the logarithmic rate of change of the carrier densities.

Proceeding as in earlier derivations [2], [3], $\alpha$ is expanded in a Taylor's series about $E_0$, to give

$$\alpha = \alpha_0 + \alpha' \Delta E + \frac{1}{2}\alpha''(\Delta E)^2$$

which means that (24) requires that

$$\alpha_0 l = 1 - \left(\frac{\alpha''}{4} - \frac{l\alpha'^2}{10}\right) E_{RF}^2 \tag{25}$$

which differs from the earlier results only by the final term, which comes from the term proportional to $\delta/5$ in (24). Thus the dc field exceeds the breakdown field by the amount

$$E_0 - E_B = \left(\frac{l\alpha'}{10} - \frac{\alpha''}{4\alpha'}\right) E_{RF}^2$$

so that the dc voltage across a punched through diode is

$$V_{dc} = V_{th}(T_j) + R_{sc} I_{dc} + \Delta V \tag{26}$$

TABLE II
Back Bias Parameters at 200°C

| $l$ ($\mu$m) | $\alpha'$ ($V^{-1}$) | $\alpha''$ ($10^{-7}$ cm/V$^2$) | $-\alpha''/4\alpha'$ ($10^{-7}$ cm/V) | $\alpha' l/10$ ($10^{-7}$ cm/V) |
|---|---|---|---|---|
| .1 | .144 | - 3.2 | 5.5 | 1.4 |
| .2 | .230 | - 1.8 | 1.9 | 4.6 |
| .3 | .232 | 1.8 | - 2.0 | 7.0 |
| .4 | .220 | 4.7 | - 5.3 | 8.8 |
| .5 | .206 | 6.8 | - 8.2 | 10.3 |

where the back bias voltage is

$$\Delta V = w_T \left(\frac{l\alpha'}{10} - \frac{\alpha''}{4\alpha'}\right) E_{RF}^2.$$

Here, $V_{th}(T_j)$ is the breakdown voltage at temperature $T_j$, $R_{sc}$ is the space charge resistance, and $w_T$ is the total width of the punched-through diode.

If the RF space charge could be neglected, $E_{RF}$ could be approximated by $V_{RF}/w_T$ where $V_{RF}$ is the peak RF voltage across the diode. More generally, by integrating Poisson's equation over the space charge moving across the diode, one can show [8], [9]

$$E_{RF} = V_{RF}/\gamma w_T$$

where $\gamma^2$ normally lies in the range $0.6 \leqslant \gamma^2 \leqslant 1.0$, and is given by

$$\gamma^2 = \left[1 - \frac{\omega_R^2}{\omega^2}\left\{\frac{w_n}{w_T}\left(1 - \frac{\sin\theta_n}{\theta_n}\right) + \frac{w_p}{w_T}\left(1 - \frac{\sin\theta_p}{\theta_p}\right)\right\}\right]^2 + \left[\frac{\omega_R^2}{\omega^2}\left\{\frac{w_n}{w_T}\left(\frac{1-\cos\theta_n}{\theta_n}\right) + \frac{w_p}{w_T}\left(\frac{1-\cos\theta_p}{\theta_p}\right)\right\}\right]^2 \tag{27}$$

where the angular resonance frequency $\omega_R^2$, the transit angles $\theta_n$ and $\theta_p$, and the drift lengths $w_n$ and $w_p$ are defined in detail elsewhere [8], [9]. Thus the back bias voltage becomes

$$\Delta V = \left(\frac{l\alpha'}{10} - \frac{\alpha''}{4\alpha'}\right) V_{RF}^2/\gamma^2 w_T. \tag{28}$$

The relative importance of the terms in (28) at 200°C is shown in Table II for different values of the avalanche width $l$. The values of $\alpha'$ and $\alpha''$ were obtained from the exponential formula $\alpha = a\exp(-(b/E)^2)$ where $a$ and $b$ at 200°C were taken as $1.81 \times 10^5$ cm$^{-1}$ and $6.33 \times 10^5$ V/cm, based on measurements taken on GaAs diodes in our laboratory [10]. According to Table II, the back bias voltage is positive for $l$ between 0.1 and 0.5 $\mu$m, even though $\alpha''$ is positive for $l$ larger than 0.25 $\mu$m.

## V. Experiment

The measurements of back bias voltage were made by operating a double-drift GaAs IMPATT diode as an amplifier in a manner similar to the conductance measurements described elsewhere [11], except that the emphasis is now on the dc voltage as a function of RF drive. In the present setup, the diode is driven by an RF voltage from a network analyzer, as indicated in the schematic diagram in Fig. 4. These measurements were made on diode 9A-98

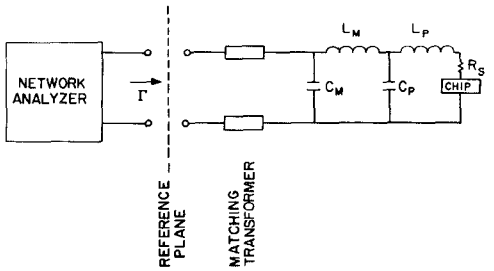


Fig. 4. Schematic diagram of the measurement circuit. The conductance and dc voltage are measured as a function of $V_{RF}$.

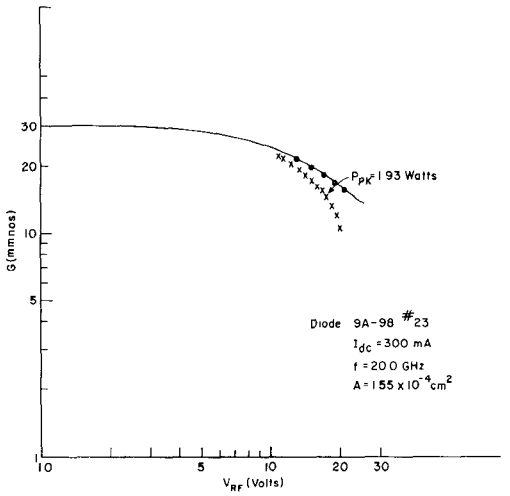


Fig. 5. Conductance versus $V_{RF}$. The crosses are measured points and should be compared with the curve calculated from an analytic model.

#23 which is designed to operate at $K$-band near 20 GHz. The parasitics involved in the transformation from the reference plane to the chip were determined experimentally. The transformation is assumed to be lossless except for the small series resistance $R_s = 0.2\ \Omega$ which was measured by the threshold method [8].

The output power and the admittance are measured at the reference plane. Using the known transformation between the reference plane and the chip, the $V_{RF}$ across the chip can then be calculated. The crosses in Fig. 5 indicate the measured values of conductance versus $V_{RF}$ for a 300-mA dc current. They can be compared with the calculated values from the analytic model [11] using the parameters listed in Table III. The relationship between the theory and measurements is similar to that observed at other frequencies [8], [9], [11], namely that the experimental measurements lie close to the analytical calculation until the conductance drops sharply when the $V_{RF}$ exceeds some critical value, which in this case is near 17 V. The assumed junction area of $1.55 \times 10^{-4}$ cm$^2$ was chosen so that the calculated susceptance would agree with the measured susceptance, but both $G$ and $\Delta V$ are insensitive to the actual value of $A$ when $I_{dc}$ is specified.

Since Section IV shows that the back bias voltage is sensitive to the avalanche width, $C-V$ measurements were taken to determine this width. The curve in Fig. 6(a), measured on a mesa from wafer 9A-98, plots $n_{\text{eff}} = n_A n_D/(n_A + n_D)$ versus the total width of the depletion regions. The maximum of $n_{\text{eff}}$, which occurs when the p-edge of the depletion region reaches the peak of the p-spike, is reached when $x_n + x_p = 0.37\ \mu$m, which is assumed to be the width of the avalanche zone. This estimate is corroborated by the $C-V$ doping profiles shown in Fig. 6(b), which were obtained by depositing Schottky barriers on the surfaces resulting from etching to different depths from the $p^+$ contact in this wafer.

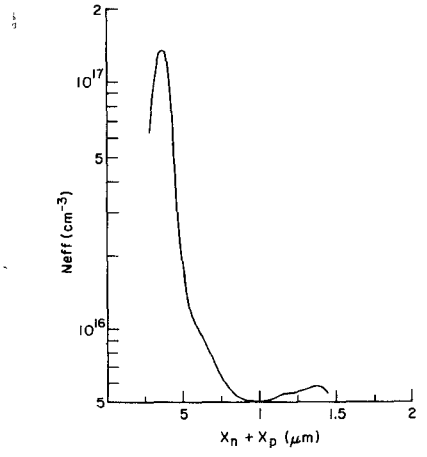


(a)

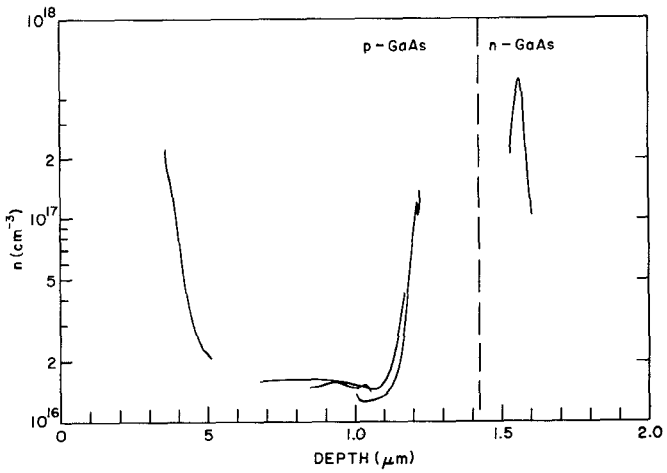


(b)

Fig. 6. (a) $N_{\text{eff}}$ versus depletion layer width for wafer 9A-98 from a mesa $C-V$ measurement.
(b) Acceptor and donor densities versus depth from Schottky barriers etched into wafer 9A-98.

TABLE III
CHARACTERISTICS OF DIODE 9A-98 #23

| | |
|---|---|
| $\ell$ = .37 μm | $w_n = w_p$ = 1.05 μm |
| θ = 19 °C/W | $\beta$ = 2.06 × $10^{-3}$ |
| $T_J$ = 200 °C | $V_B$ (25 °C) = 21.8 V |
| $\alpha'$ = .224 $V^{-1}$ | $\alpha''$ = 3.9 × $10^{-7}$ cm $V^{-2}$ |
| f = 20 GHz | A = 1.55 × $10^{-4}$ $cm^2$ |
| $v_n = v_p$ = 4.7 × $10^6$ cm/sec | $w_T$ = 2.09 μm |

The dc voltage was measured as a function of $V_{RF}$ at the same time as the output power and the conductance was measured at 300-mA dc current. Knowing the dissipated power and the measured value of thermal resistance in

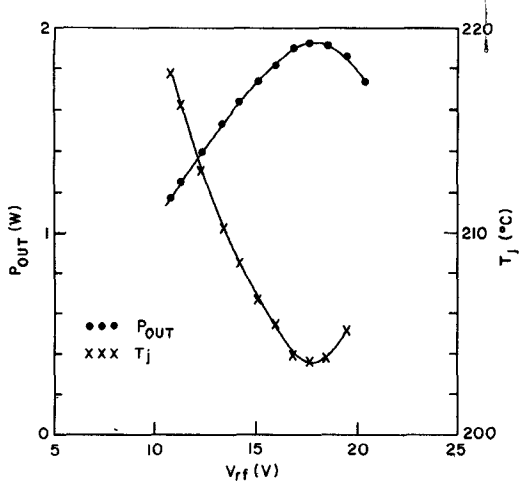


Fig. 7. $P_{out}$ and $T_j$ versus $V_{RF}$. $T_j$ is calculated from electrical measurements using the measured value of thermal resistance.

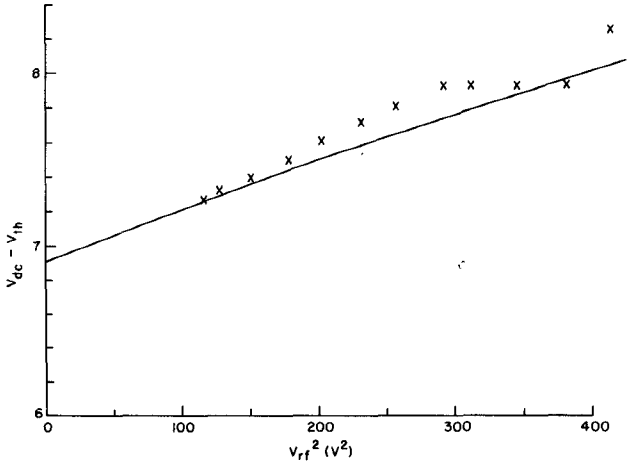


Fig. 8. $V_{dc} - V_{th}$ versus $V_{RF}^2$. The curve is an assumed value of $R_{sc}I_{dc}$ plus the calculated value of $\Delta V$.

Table III, the junction temperature was calculated as a function of $V_{RF}$ as plotted in Fig. 7. The changes in dc voltage are less important than the drop in temperature caused by radiating more power out as $V_{RF}$ increases toward the maximum output power point at 17.6 V.

The breakdown voltage at temperature $T$ is calculated from the relationship $V_{th} = V_B(1 + \beta\Delta T_j)$ where $\beta$ has the measured value given by Table III. Thus the measured values of $V_{dc} - V_{th}$ can be plotted versus $V_{RF}^2$ as shown by the crosses in Fig. 8.

According to (26), $V_{dc} - V_{th}$ should equal $R_{sc}I_{dc} + \Delta V$ where $\Delta V$ is given by (28). This function is plotted as the solid curve in Fig. 8 where $R_{sc}$ is arbitrarily taken as 23 Ω. The precise value of $R_{sc}$ is not important since $I_{dc}$ is kept constant so that we are mainly interested in the slope of $\Delta V$ versus $V_{RF}^2$, which is given by the coefficient of $V_{RF}^2$ in (28). Note that $R_{sc}$ will increase by a negligible amount with $V_{RF}^2$ since the change in saturated velocity is small for the temperature change shown in Fig. 7.

If we use the simplified formula

$$R_{sc} = \frac{1}{2\epsilon A_{\text{eff}}}\left(\frac{w_n^2}{v_n} + \frac{w_p^2}{v_p}\right) \tag{29}$$

the value of $A_{\text{eff}}$ needed to give 23 Ω is $0.92\times10^{-4}$ cm$^2$, which corresponds to 60 percent of our assumed junction area of $1.55\times10^{-4}$ cm$^2$. This ratio is comparable to the ratios $A_{\text{eff}}/A$ noted by other experimenters and attributed to nonuniform current distribution.

The slope of the experimental points in Fig. 8 is positive and quite close to the curve calculated from (28). The main deviation occurs with the last four points, which correspond to $V_{RF}$ greater than 17 V, which is where the analytical model is already known to break down as shown by Fig. 5. The curve calculated for the back bias voltage in Fig. 8 bends downward slightly from a straight line because $\gamma^2$ increases from 0.56 when $V_{RF} = 0$ to 0.72 when $V_{RF} = 20$.

## VI. Saturation Current Effects

Saturation current provides a mechanism which can cause a negative back bias voltage at low frequencies and large $V_{RF}$. Although saturation current is unimportant under the conditions in which our measurements were made, its effect at lower frequencies can be quickly derived from formulas given by Statz *et al.* [12]. Equation (2) of [12] defines a quantity $A$ such that

$$\Delta V = \frac{w_T\omega\tau_i}{\alpha' l}A. \tag{30}$$

Under the condition that $I_{sat} \ll I_{dc}$, which would generally hold for a practical IMPATT diode, one can show that, for $q = 0$, (7) of [12] requires that

$$A = \frac{1}{\omega\tau_i}\frac{I_{sat}}{I_{dc}}[I_0(B)]^2 \tag{31}$$

where, in our notation

$$B = \frac{3\alpha' v}{\omega w_T \gamma}V_{rf}, \text{ and } I_0(B) \text{ is}$$

the modified Bessel function.

Combining (30) and (31) gives the saturation cuRent contribution to the back bias voltage. Since the analysis oF [12] leaves Out the effect of $\alpha''$ and the modulation of $\tau_i$, the total back bias voltage will also include the terms from (28), giving

$$\Delta V = -\frac{w_T}{\alpha' l}\frac{I_{sat}}{I_{dc}}[I_0(B)]^2 + \left(\frac{l\alpha'}{10} - \frac{\alpha''}{4\alpha'}\right)V_{RF}^2/\gamma^2 w_T. \tag{32}$$

Because $B$ is inversely proportional to frequency and the modified Bessel function increases exponentially with $B$ for large $B$, the saturation current contribution to (32) will dominate at low frequencies even for quite small saturation currents. As a numerical example, we choose the same diode used by Blakey *et al.* [4] to compute the back bias voltage obtained by numerical simulation and shown in [4, Fig. 6]. In this example, $w_T = 4.9$ μm and $l = 0.45$ μm. Taking $\gamma \simeq 1$, $v$ from Table III, $\alpha' = 0.213$, and $\alpha'' = 6.8\times10^{-7}$ (from Table II), the back bias voltage was calculated from (32) and plotted in Fig. 9, assuming $I_{sat}/I_{dc} = 10^{-4}$. Qualitatively, these results are like [4], although an exact comparison cannot be made since [4] did not specify the

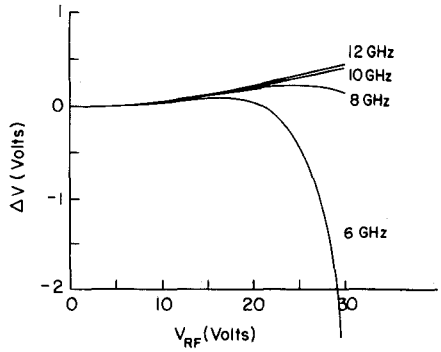


Fig. 9. Back bias voltage versus $V_{RF}$ with frequency as a parameter. The calculations are for the same diode parameters as the numerical simulation in [5].

saturation current used in their simulation. Moreover, our assumption that $\gamma \simeq 1$ would not be fully justified for their current density of 500 A/cm$^2$ because $\gamma$ would equal 0.72 at 6 GHz with $V_{RF} = 30$ V. (In practice, the diode would be operated at a lower current density at 6 GHz since the avalanche frequency, 5.8 GHz, is nearly as large as the operating frequency.)

The saturation current effect can be understood by realizing that it prevents the avalanche current from dropping below $I_{sat}$ when the RF voltage is negative; since the current increase is not constrained when the RF voltage is positive, the dc voltage must be reduced to keep the net current increase over a cycle equal to zero. At high frequencies, the effect is unimportant since there is not enough time for the current to drop from dc levels to a level near $I_{sat}$. This effect will become more important at high powers because the saturation current increases exponentially with temperature.

## VII. Conclusion

A calculation of the carrier densities in a Read avalanche zone was carried out to the second order in $\delta$. It was shown that this term modifies the derivation of the back bias voltage by adding a term which is always positive and often larger than the term due to $\alpha''$. An experimental measurement verified this effect by showing a positive back bias for an avalanche zone width which would have required a negative back bias voltage according to the older theory of (1). Thus the back bias voltage should not drive low-frequency instabilities [1] under conditions in which the saturation current is negligible. However, at low frequencies and high saturation currents, $V_{bb}$ will become negative for sufficiently large $V_{RF}$.

## Acknowledgment

We thank Dr. J. McClymonds for advice on microwave measurements, Dr. H. Statz and Dr. M. G. Adlerstein for discussions on back bias voltage and the materials characterization laboratory for $C-V$ measurements.

## References

[1] Y. Hirachi, T. Nakagami, Y. Toyama, and Y. Fukukawa, "High-power 50-GHz double-drift-region IMPATT oscillators with improved bias circuits for eliminating low-frequency instabilities," *IEEE Trans. Microwave Theory Tech.*, vol. MTT-24, pp. 731–737, Nov. 1976.

[2] B. Culshaw, R. A. Giblin, and P. A. Blakey, "Avalanche diode oscillators II. Capabilities and limitations," *Int. J. Electron.*, vol. 39, pp. 121–172, 1975.

[3] J. J. Goedbloed, "Noise in IMPATT-diode oscillators," M.S. thesis, Technological University Eindhoven, 1973; also *Philips Res. Rep. Suppl.*, no. 7, 1973.

[4] P. A. Blakey, B. Culshaw, and R. A. Giblin, "Comprehensive models for the analysis of high-efficiency GaAs IMPATT's", *IEEE Trans. Electron Devices*, vol. ED-25, pp. 674–682, June 1978.

[5] W. T. Read, Jr., "A proposed high-frequency negative resistance diode," *Bell Syst. Tech. J.*, vol. 37, pp. 401–444, Mar. 1958.

[6] R. Kuvas and C. A. Lee, "Quasistatic approximation for semiconductor avalanches," *J. Appl. Phys.*, vol. 41, pp. 1743–1755, 1970.

[7] L. H. Holway, Jr., "Electron-hole avalanches with constant ionization efficients," *IEEE Trans. Electron Devices*, vol. ED-26, pp. 991–993, June 1979.

[8] M. G. Adlerstein, L. H. Holway, and G. S. L. Chu, "Measurement of series resistance in IMPATT diodes," *IEEE Trans. Electron Devices*, vol. ED-30, pp. 179–182, Feb. 1983.

[9] L. H. Holway, Jr. and G. S. L. Chu, "Broad-band characteristics of EHF IMPATT diodes," *IEEE Trans. Microwave Theory Tech.*, vol. MTT-30, pp. 1933–1939, Nov. 1982.

[10] L. H. Holway, Jr., S. R. Steele, and M. G. Adlerstein, "Measurement of electron and hole properties in p-type GaAs," in *Proc. Seventh Biennial Conf. Active Microwave Semiconductor Devices and Circuits*, Cornell Univ., 1979, pp. 199–208.

[11] M. G. Adlerstein, J. W. McClymonds, and H. Statz, "Avalanche response time in GaAs as determined from microwave admittance measurements," *IEEE Trans. Electron Devices*, vol. ED-28, pp. 808–811, July 1981.

[12] H. Statz, R. A. Pucel, J. E. Simpson, and H. A. Haus, "Noise in gallium arsenide avalanche Read diodes," *IEEE Trans. Electron Devices*, vol. ED-23, pp. 1075–1085, Sept. 1976.

**Lowell H. Holway, Jr.** was born in St. Louis, Mo. He received the A.B. degree in mathematics (summa cum laude) from Dartmouth College, Hanover, NH, in 1953. Subsequently, he received the M.A. degree in physics and the Ph.D. degree in applied mathematics from Harvard University, Cambridge, MA, in 1955 and 1964, respectively.

Since 1955, he has been employed at the Raytheon Company where he is presently a Principal Research Scientist. At Raytheon, he has been involved in computational physics of a variety of physical problems, such as the modification of the ionosphere by high-power HF transmissions and the breakdown of insulating crystals by intense laser beams. Since 1974, he has been involved with modeling the device physics of IMPATT diodes and field effect transistors. He has supervised measurements of trap lifetimes by DLTS and PITS experiments and the measurement of ionization coefficients and hole velocities in GaAs, and has been involved in studies of the relationship of midgap states to SI GaAs. He is the author or coauthor of 33 publications in books or journals and has given 22 talks at meetings and symposia.

Dr. Holway is a member of the American Physical Society and Phi Beta Kappa.

**Shiou Lung G. Chu** was born in London, England. She received the B.S. degree in physics from Fu-Jen University in Taipei, Taiwan, in 1971, and the M.A. degree, also in physics, from Boston University in Boston, MA, in 1973.

She joined the Raytheon Research Division, Lexington, MA, in 1973. She has worked on silicon TRAPATT and Gunn devices, GaAs IMPATT oscillators, and combiners. Since 1978, she has been engaged in the research and development of millimeter-wave GaAs IMPATT diodes and circuits. She is a Senior Scientist and is cuRently working on pulsed IMPATT diodes.